Proceedings of ASME Turbo Expo 2011
GT2011
June 6-10, 2011, Vancouver, British Columbia, Canada

GT2011-46286

NONLINEAR DYNAMIC ANALYSIS OF A MULTI-GEAR TRAIN WITH TIME-VARYING MESH STIFFNESS INCLUDING MODIFICATION COEFFICIENT EFFECT

T. N. Shiau *, Professor
J. R. Chang **, Associate Professor
K. H. Huang***, Manager
C. J. Cheng***, Engineer
C. R. Wang***, Engineer

* Department of Mechanical Engineering
National Chung Cheng University
621 Chia Yi, Taiwan, R.O.C.
E-mail:imetls@gmail.com

** Department of Mechanical Engineering
Air Force Institute of Technology
820 Kaohsiung, Taiwan, R.O.C.

***FATEK Automation Technology Co., Ltd.
621 Chia-Yi, Taiwan, R.O.C.
E-mail:rotorsystem@yahoo.com.tw

ABSTRACT

The nonlinear dynamic analysis of a multi-gear train with time-varying mesh stiffness on account of the modification coefficient effect is investigated in this paper. The proposed application of the modification coefficient will revise the center distance of the gear pair, avoid undercut and raise the mesh stiffness of the designed gear system. In this study, the gear profile is generated from the relationship between the rack cutter and the gear work piece by using the envelope theory. The rack cutter with the modification coefficient increases the mesh stiffness and thus enhances the strength of the gear tooth. Then the time-varying mesh stiffness at the contact position of the gear pair is calculated from the tooth deflection analysis using the generated gear profile. With the obtained time-varying mesh stiffness, the nonlinear dynamic behavior of multi-gear train is investigated by using Runge-Kutta integration method. The numerical results of the studied examples show the harmonic motion, sub-harmonic motion, chaotic motion and bifurcation phenomenon of the gear train.

Keywords: modification coefficient, gear train, time-varying stiffness, rack cutter, bifurcation diagram, nonlinear dynamic.

I. INTRODUCTION

In the gear systems groups, Ozguven and Houser [1] defined the mathematical models of gear dynamics and discussed the dynamic loads of effects including tooth error, addendum modification, mesh stiffness, damping factor and friction coefficient Kahraman and Singh [2] developed a single gear pair model which includes the nonlinearities associated with radial clearances in rolling element bearings and backlash between a spur gear pair. Kahraman and Singh [3] also developed a 3DOF time-varying model with a single gear pair which includes the radial clearances between bearings and backlash of gear pair. Sener and Ozguven [4] used a continuous system model to study the dynamic mesh force and dynamic factor with a geared shaft system.

The nonlinear vibration of a spur gear pair with flexible shaft is investigated by Litak and Friswell [5]. Two years later, Al-shyyab and Kahraman [6] proposed a nonlinear time-varying dynamic model with three shaft and two gear pairs. The system was reduced two degree of freedom and definite model by using the relative gear mesh displacements as the coordinates and assuming rigid shafts. At the same year, Al-shyyab and Kahraman [7] used the same model to obtain the steady state period-n sub-harmonic motions and the Floquet theory which applied to determine the stability of the steady state solutions. Zhao and Sun [8] used the a nonlinear spur gear models to investigate the chaos and bifurcation, and discussed the influence of mesh frequency, amplitude of mesh stiffness and damping ratio on nonlinear dynamic behavior.

In the mesh stiffness method groups, Cornell and Westervelt [9] presented the closed form solution of a dynamic model of spur gear system with all practical contact ratios. Cornell [10] obtained a relationship between compliance and stress sensitivity of spur gear teeth. The different magnitude of the tooth pair compliance with load position affected the dynamics and loading significantly. Yoon and Rao [11] proposed a new tooth profile, and presented as the cubic splines and compared the dynamic factor and tooth load with involute profile, the new profile can be minimized the static transmission error, gear vibration and noise. An original analytical modeling of tooth cracks is presented by Chaari, Fakhfakh and Haddar [12]. The gear mesh stiffness reduction due to the tooth crack is quantified and compared the results with the finite element model to validate this analytical formulation.

Researchers usually use contact value, multi-term Fourier series and periodic rectangular wave to approximate mesh stiffness, but it was not real meshing condition by involute tooth profile. Though the past researches have predicted the gear mesh stiffness, the generation of spur gear tooth profile using rack cutter with modification coefficient is proposed in this study. The real involute tooth profile and formulation is extendable developed the proposed method of reference [13]. The nonlinear dynamic behavior of the associated gear train system is also investigated based on the predicted gear mesh stiffness in this study.

Ⅱ. DYNAMIC MODEL FORMULATION

A physical model of a multi-degree-of-freedom nonlinear time-varying system (Al-shyyab and Kaharman [6]) is investigated as shown in Fig. 1. The torsional system is formed by three rigid shafts connected to each other by two spur gear pairs. Shafts are assumed to be rigid such that no deflection in any direction is possible. Gears are connected to the shafts rigidly. Bearings are also considered to be rigid and gear mesh damping values are assumed to be time-varying. The focus of this study is on the dynamic transmission error and modification coefficient.

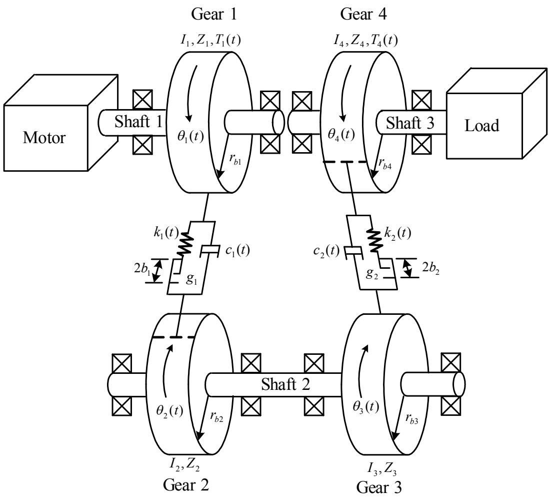

Figure 1 Dynamic model of the physical system

The number of tooth in each gear is Z_i. The polar mass moment of inertia is I_i. The base radius is r_{bi}. $\theta_i(t)$ represents the rotational displacement of each gear. $k_1(t)$ and $k_2(t)$ represent gear mesh stiffness of the first and second gear pair. The gear mesh damping values are denoted by $c_1(t)$ and $c_2(t)$. $g_1(t)$ and $g_2(t)$ are discontinuous displacement function due to the gear backlash.

Since the shafts are assumed rigid, the torsional displacements of gear 2 and gear 3 are equal, i.e., $\theta_2(t) = \theta_3(t)$, and the associated polar mass moment of inertia becomes $I_{23} = I_2 + I_3$. The number of equations of motion can be reduced to two by defining the following equations

$$p_1(t) = r_{b1}\theta_1(t) - r_{b2}\theta_2(t) \tag{1}$$

$$p_2(t) = r_{b3}\theta_2(t) - r_{b4}\theta_4(t) \tag{2}$$

where $p_1(t)$ and $p_2(t)$ are the dynamic transformation error.

Substituting the kinetic and potential energy into the Lagrange approach, one can obtain the dimensionless equations as follows

$$\begin{Bmatrix}\ddot{\bar{p}}_1(\bar{t})\\ \ddot{\bar{p}}_2(\bar{t})\end{Bmatrix} + 2\begin{bmatrix}\zeta_{11}(\bar{t}) & -\zeta_{12}(\bar{t})\\ -\zeta_{21}(\bar{t}) & \zeta_{22}(\bar{t})\end{bmatrix}\begin{Bmatrix}\dot{\bar{p}}_1(\bar{t})\\ \dot{\bar{p}}_2(\bar{t})\end{Bmatrix} + \begin{bmatrix}\kappa_{11}(\bar{t}) & -\kappa_{12}(\bar{t})\\ -\kappa_{21}(\bar{t}) & \kappa_{22}(\bar{t})\end{bmatrix}\begin{Bmatrix}\bar{g}_1(\bar{t})\\ \bar{g}_2(\bar{t})\end{Bmatrix} = \begin{Bmatrix}f_1(\bar{t})\\ f_2(\bar{t})\end{Bmatrix} \tag{3}$$

where

$$m_1 = \frac{I_1 I_{23}}{r_{b1}{}^2 I_{23} + r_{b2}{}^2 I_1},\ m_2 = \frac{I_{23}}{r_{b2} r_{b3}},\ m_3 = \frac{I_{23} I_4}{r_{b4}{}^2 I_{23} + r_{b3}{}^2 I_4},$$

$$\kappa_{11}(\bar{t}) = \frac{k_1(\bar{t})}{m_1\omega_c^2},\ \kappa_{12}(\bar{t}) = \frac{k_2(\bar{t})}{m_2\omega_c^2},\ \kappa_{21}(\bar{t}) = \frac{k_1(\bar{t})}{m_2\omega_c^2},\ \kappa_{22}(\bar{t}) = \frac{k_2(\bar{t})}{m_3\omega_c^2}$$

$$\zeta_{11}(\bar{t}) = \frac{c_1(\bar{t})}{2m_1\omega_c},\ \zeta_{12}(\bar{t}) = \frac{c_2(\bar{t})}{2m_2\omega_c},\ \zeta_{21}(\bar{t}) = \frac{c_1(\bar{t})}{2m_2\omega_c},\ \zeta_{22}(\bar{t}) = \frac{c_2(\bar{t})}{2m_3\omega_c}$$

Consider a dimensionless time $\bar{t} = t\,\omega_c$, where t is real time, ω_c is the characteristic frequency, and then let $\bar{b}_i = b_i / b_c\ (i, j = 1,2)$, where b_c is a characteristic length. The mesh damping value $c_1(\bar{t})$, $c_2(\bar{t})$ are defined as $c_1(\bar{t}) = 2\zeta\sqrt{k_1(t)m_{12}}$ and $c_2(\bar{t}) = 2\zeta\sqrt{k_2(\bar{t})m_{34}}$, where the equivalent mass are $m_{12} = I_1 I_2 / (r_{b1}{}^2 I_2 + r_{b2}{}^2 I_1)$, $m_{34} = I_3 I_4 / (r_{b3}{}^2 I_4 + r_{b4}{}^2 I_3)$, and ζ is the damping ratio.

Dimensionless discontinuous displacement function and external force are given as

$$\bar{g}_i(\bar{t}) = \begin{cases}\bar{p}_i(\bar{t}) - \bar{b}_i & \bar{p}_i(\bar{t}) > \bar{b}_i\\ 0 & if\ \left|\bar{p}_i(\bar{t})\right| \le \bar{b}_i\ \ i = 1,2\\ \bar{p}_i(\bar{t}) + \bar{b}_i & \bar{p}_i(\bar{t}) < -\bar{b}_i\end{cases} \tag{4}$$

and

$$f_1(\bar{t}) = \frac{r_{b1}T_1(\bar{t})}{I_1\omega_c^2 b_c} \quad \text{and} \quad f_2(\bar{t}) = \frac{r_{b4}T_4(\bar{t})}{I_4\omega_c^2 b_c} \tag{5}$$

where $\bar{p}_i(\bar{t}) = \dfrac{p_i(\bar{t})}{b_c}$ is the dimensionless dynamic transformation error.

Ⅲ. GENERATION OF PROFILE AND TIME-VARYING MESH STIFFNESS WITH MODIFICATION COEFFICIENT

Modification Coefficient

The modification coefficient has three limitations including the undercut of tooth (x_u), the tip of tooth profile (x_t) and the limited region of modification coefficient. These limitations are defined in the following equations.

$$x_u = \frac{z_{\lim} - z}{z_{\lim}},\quad z_{\lim} = fix\left(\frac{2}{\sin^2\alpha_c}\right) \tag{6}$$

To avoid producing the acute top of tooth profile, the tip of the tooth profile is given as

$$x_t = \frac{inv(\alpha_k) - inv(\alpha_c)}{2z\tan(\alpha_c)} - \frac{\pi}{4\tan(\alpha_c)} \tag{7}$$

where

$$\alpha_k = \cos^{-1}\left(\frac{r_b}{r_p + h_f + x_t.m}\right) \tag{8}$$

Therefore, the limitation region of modification coefficient is written as

$$x_u < x < x_t \tag{9}$$

It is noted that the modification coefficient x should be larger than x_u to avoid the undercut of tooth and less than x_t to avoid producing the acute top of tooth profile.

In Eqns. (6)-(8), z is the number of tooth, $z_{\lim}$ is the limiting number of tooth of undercut, α_c is the pressure angle of rack cutter, fix(i) is the maximum integral value of i, $inv(\theta) = \tan(\theta) - \theta$ is the involute function, α_k is the meshing angle, m, r_b, r_p, and h_f are the modulus, radius of base circle, radius of pitch circle and addendum of the gear, respectively.

Formulation of Rack Cutter

The rack cutter consists of a straight line section and arc section. In Fig. 2, the form of cutter vector is defined by

$$\mathbf{r}_1^{(1)} = \left[\pm(u_1\sin\alpha - t_f\tan\alpha - \frac{t_0}{2}) \quad u_1\cos\alpha - t_f + x\cdot m \quad 1\right]^T \tag{10}$$

$$\mathbf{r}_1^{(2)} = \left[\pm(-\frac{t_0}{2} - t_f\tan\alpha - \rho\cos\alpha - \rho\cos\theta_1) \quad -t_f + \rho\sin\alpha + \rho\sin\theta_1 + x\cdot m \quad 1\right]^T \tag{11}$$

where α is the pressure angle, ρ is the radius of fillet, x is modification coefficient. u_1 and θ_1 are the parameters of straight line section and arc section of tooth profile, respectively. Likewise, the superscripts (1) and (2) describe the straight line and the arc section, respectively. The + and – signs stand for the left and right hand side of rack cutter, respectively. t_f and c_k represent the dedendum and clearance. t_0 is standard pitch.

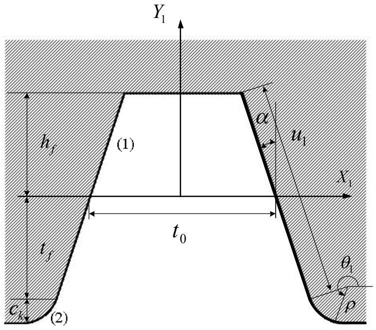

Figure 2 The rack cutter model at S_1 (X_1, Y_1) coordinate

Coordinate System & Contact Definition

In Fig. 3, S_f (X_f , Y_f) is the fixed coordinate, S_1 (X_1, Y_1) is the horizontal moving coordinate of cutter, and S_2 (X_2 , Y_2) is the rotational coordinate of gear. ϕ is the rotational angle of gear, and r_p is the radius of pitch circle. The transformation matrix of S_1 to S_2 can be presented as

$$[M_{21}] = \begin{bmatrix} \cos\phi & \sin\phi & r_p(\sin\phi - \phi\cos\phi) \\ -\sin\phi & \cos\phi & r_p(\cos\phi + \phi\sin\phi) \\ 0 & 0 & 1 \end{bmatrix} \tag{12}$$

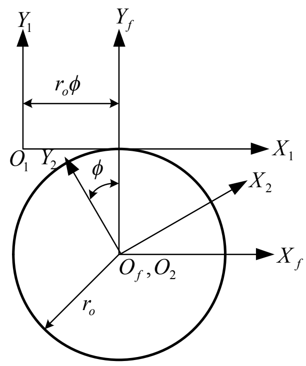

Figure 3 Coordinate transformation model

According to Eq. (12), the position vector $\mathbf{r}_2$ of the rack cutter at S_2 coordinate system can be obtained as

$$\mathbf{r}_2^{(1)} = [M_{21}]\,\mathbf{r}_1^{(1)} \text{ and } \mathbf{r}_2^{(2)} = [M_{21}]\,\mathbf{r}_1^{(2)} \tag{13}$$

where

$$\mathbf{r}_2^{(1)} = \begin{bmatrix} \lambda_1\sin\phi + r_p(\sin\phi - \phi\cos\phi) \pm \lambda_2\cos\phi \\ \lambda_1\cos\phi + r_p(\cos\phi + \phi\sin\phi) \mp \lambda_2\sin\phi \\ 1 \end{bmatrix} \tag{14}$$

$$\mathbf{r}_2^{(2)} = \begin{bmatrix} \lambda_3\sin\phi + r_p(\sin\phi - \phi\cos\phi) \pm \lambda_4\cos\phi \\ \lambda_3\cos\phi + r_p(\cos\phi + \phi\sin\phi) \mp \lambda_4\sin\phi \\ 1 \end{bmatrix} \tag{15}$$

and

$$\lambda_1 = -t_f + u_1\cos\alpha + x\cdot m$$

$$\lambda_2 = -\frac{t_0}{2} + u_1\sin\alpha - t_f\tan\alpha$$

$$\lambda_3 = \rho\sin\alpha + \rho\sin\theta_1 - t_f + x\cdot m$$

$$\lambda_4 = -\rho\cos\alpha - \rho\cos\theta_1 - \frac{t_0}{2} - t_f\tan\alpha$$

Eqns. (14) and (15) presented the equation of orbit of rack cutter on the S_2 coordinate. According to the envelop theory, the tangent vector of the equation of rack cutter is perpendicular to the normal vector of gear profile, therefore, the necessary condition of envelop is expresses as

$$\frac{\partial}{\partial\phi}\left(\mathbf{r}_2^{(1)}(u,\phi) + \mathbf{r}_2^{(2)}(\theta,\phi)\right)\cdot\left[\frac{\partial}{\partial u}\mathbf{r}_2^{(1)}(u,\phi) + \frac{\partial}{\partial\theta}\mathbf{r}_2^{(2)}(\theta,\phi)\right]\times\vec{k} = 0 \tag{16}$$

The Eq. (16) provides two independent equations to obtain the rotational angles $\phi^{(1)}$ and $\phi^{(2)}$. Substituting the rotational angle into Eqns. (14) and (15), one obtain the equations of profile $\mathbf{r}_2$ as

$$\mathbf{r}_2^{(involute)} = \left[\pm(a_1\cos a_2 + a2\sin a_2) \quad -a_1\sin a_2 + a_3\cos a_2 \quad 1\right]^T \tag{17}$$

$$\mathbf{r}_2^{(fillet)} = \left[\pm(b_1\cos b_2 + b_3\sin b_2) \quad -b_1\sin b_2 + b_3\cos b_2 \quad 1\right]^T \tag{18}$$

where

$$a_1 = \left(3x - t_f\right)\cot\alpha + u\cos^2\alpha$$
$$a_2 = \frac{1}{r_p}\left(\frac{t_0}{2} + t_f \sec\alpha\csc\alpha - u\csc\alpha - 3x\cot\alpha\right)$$
$$a_3 = u\cos\alpha - t_f + 3x + r_p$$
$$b_1 = \left(3x - t_f\right)\cot\theta + \rho\cos\theta\left(1 + \sin\alpha\csc\theta\right)$$
$$b_2 = \frac{1}{r_p}\left[\frac{t_0}{2} + t_f\left(\tan\alpha + \cot\theta\right) + \rho\sin\alpha\left(\cot\alpha - \cot\theta\right) - 3x\cot\theta\right]$$
$$b_3 = \rho\left(\sin\alpha + \sin\theta\right) - t_f + 3x + r_p$$

The mesh condition is used to obtain the equation of line of action, the normal vectors of rack cutter is first derived as

$$\mathbf{N}_1^{(1)} = \frac{\partial \mathbf{r}_1^{(1)}}{\partial u_1} \times \mathbf{k}\ ,\quad \mathbf{N}_1^{(2)} = \frac{\partial \mathbf{r}_1^{(2)}}{\partial \theta_1} \times \mathbf{k} \tag{19}$$

And the associated unit normal vectors are

$$\mathbf{n}_1^{(1)} = \begin{bmatrix}\cos\alpha & \pm(-\sin\alpha) & 0\end{bmatrix}^T$$
$$\mathbf{n}_1^{(2)} = \begin{bmatrix}\cos\theta_1 & \pm(-\sin\theta_1) & 0\end{bmatrix}^T \tag{20}$$

The unit normal vector of rack cutter at S_2 coordinate system can be obtained as

$$\mathbf{n}_2^{(1)} = [M_{21}]\mathbf{n}_1^{(1)} = \begin{bmatrix}\cos\alpha\cos\phi \mp \sin\alpha\sin\phi \\ \pm(-\cos\phi\sin\alpha) - \cos\alpha\sin\phi \\ 0\end{bmatrix} \tag{21}$$

$$\mathbf{n}_2^{(2)} = [M_{21}]\mathbf{n}_1^{(2)} = \begin{bmatrix}\cos\theta_1\cos\phi \mp \sin\theta_1\sin\phi \\ \pm\left(-\cos\phi\sin\theta_1 - \cos\theta_1\sin\phi\right) \\ 0\end{bmatrix} \tag{22}$$

Using Eqns. (13) to (18), one can obtain the unit normal vectors of gear profile on S_2 coordinate as follows

$$\mathbf{n}_2^{(involute)} = \begin{bmatrix}\cos(a_2 - \alpha) & \mp\sin(a_2 - \alpha) & 0\end{bmatrix}^{\mathrm{T}} \tag{23}$$
$$\mathbf{n}_2^{(fillet)} = \begin{bmatrix}\cos(b_2 - \theta_1) & \pm\sin(b_2 - \alpha) & 0\end{bmatrix}^T \tag{24}$$

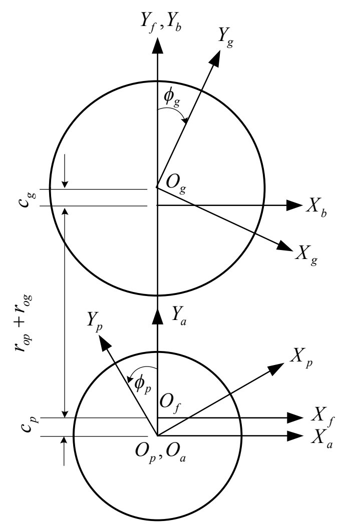

Figure 4 Gear meshing coordinate system

The gear pair including pinion "p" and gear "g" is shown in Fig. 4. r_{op} and r_{og} are the radii of pitch circle. ϕ_p and ϕ_g are the rotational angles of pinion and gear. c_p and c_g are displacements of center distance. In the gear mesh coordinate system, S_p , S_g and S_f are rotational coordinates of pinion and gear, and fixed coordinate. S_a and S_b are parallel moving coordinates of pinion and gear. The tooth profile vector of pinion $\mathbf{r}_{fp}^{(1)}$ and unit normal vector $\mathbf{n}_p^{(1)}$ at S_f coordinate system can be represented as

$$\mathbf{r}_{fp}^{(i)} = [M_{fp}]\,\mathbf{r}_{2p}^{(i)},\ \ \mathbf{n}_{fp}^{(i)} = [M_{fp}]\,\mathbf{n}_{2p}^{(i)}\ ,\ i\text{=}1,\ 2 \tag{25}$$

where

$$[M_{fp}] = \begin{bmatrix}\cos\phi_p & -\sin\phi_p & 0 \\ \sin\phi_p & \cos\phi_p & -c_p \\ 0 & 0 & 1\end{bmatrix} \tag{26}$$

Similarly, the tooth profile vector of gear $r_{fg}^{(1)}$ and unit normal vector $n_{fg}^{(1)}$ at S_f coordinate system are

$$\mathbf{r}_{fg}^{(i)} = [\mathrm{M}_{fg}]\ \mathbf{r}_{2g}^{(i)},\ \ \mathbf{n}_{fg}^{(i)} = [\mathrm{M}_{fg}]\ \mathbf{n}_{2g}^{(i)},\ i\text{=}1,\ 2 \tag{27}$$

When two gears are meshed, the contact points is concurrent and normal vectors is collinear. These conditions can be restrained by the following constraints.

$$\left|r_{fp}^{(1)}\right| = \left|r_{fg}^{(1)}\right|,\ \left|n_{fp}^{(1)}\right| = \left|n_{fg}^{(1)}\right| \tag{28}$$

If the rotational angle of pinion ϕ_p is given, then, the position of any point on line of action and contact length can be determined.

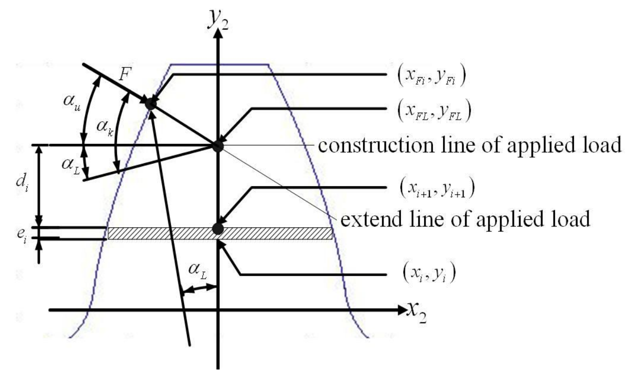

Figure 5 Beam, fillet and foundation compliance of a gear tooth

Deflection

According to Cornell's research [10], the formulation of compliance of spur gear is applied. The total deflection of single tooth includes three parts: (1) the involute deflection δ_{inv} and fillet deflection δ_{fillet} of tooth；(2) the foundation deflection δ_F ；(3) the Hertz contact deflection δ_H .

$$\delta_{total} = \delta_p + \delta_g + \delta_H \tag{29}$$

where

$$\begin{aligned}\delta_p &= \left(\delta_{inv}\right)_p + \left(\delta_{fillet}\right)_p + \left(\delta_F\right)_p \\ \delta_g &= \left(\delta_{inv}\right)_g + \left(\delta_{fillet}\right)_g + \left(\delta_F\right)_g\end{aligned} \tag{30}$$

Involute and Fillet Deflection

To calculate the deflection of tooth δ_{inv} and δ_{fillet}, the tooth is divided into a sequence of segments and each segment is regarded as a cantilever beam. For each segment *i*, the average value at both faces is uses as the height on profile $\bar{h}_i$, the cross-sectional area $\bar{A}_i$ and the area moment on inertia $\bar{I}_{Ai}$ are used the average values at both faces:

$$\bar{h}_i = \left(h_i + h_{i+1}\right)/2 \tag{31}$$

$$\bar{A}_i = \left(A_i + A_{i+1}\right)/2 \tag{32}$$

$$\bar{I}_{Ai} = \left(I_{Ai} + I_{Ai+1}\right)/2 = W\left(y_i^3 + y_{i+1}^3\right)/3 \tag{33}$$

Figure 5 shows three vectors: (1) the vector of applied load $\left(x_{Fi}, y_{Fi}\right)$, (2) the vector of construction line of applied load $\left(x_{FL}, y_{FL}\right)$, (3) the vector of segments $\left(x_i, y_i\right)$. The deflection of tooth is calculated by using the following equations.

$$\delta_{inv} = \frac{F\cos^2\alpha_u}{WE_e}\sum_{i=1}^{j} e_i\left\{\frac{d_i^2 - d_i e_i + e_i^2/3}{\bar{I}_{Ai}} + \frac{2.4(1+\nu)+\tan^2\alpha_k}{\bar{A}_i}\right\} \tag{34}$$

$$\delta_{fillet} = \frac{F\cos^2\alpha_u}{WE_e}\sum_{i=1}^{o} e_{fi}\left\{\frac{d_{fi}^2 - d_{fi} e_{fi} + e_{fi}^2/3}{\bar{I}_{Afi}} + \frac{2.4(1+\nu)+\tan^2\alpha_k}{\bar{A}_{fi}}\right\} \tag{35}$$

where F is applied load, W is gear width, E_e is equivalent elastic modulus, ν is Poisson's ratio and α_u is angle of applied load. j and o represent the number of segment for involute and fillet. d_i and d_{fi} represent distance from segment to construction line of applied load for involute and fillet. e_i and e_{fi} are represented segment width for involute and fillet, respectively. Besides, α_u, d_i and e_i are given as follows

$$\alpha_u = \alpha_k - \alpha_L \tag{36}$$

$$d_i = y_{FL} - y_i \tag{37}$$

$$e_{fi} = y_{i+1} - y_i \tag{38}$$

α_k is meshing angle. α_L is angle between y-axis and radial line to the contact point. $y_{FL} = y_{Fi} - x_{Fi}\tan\alpha_u$.

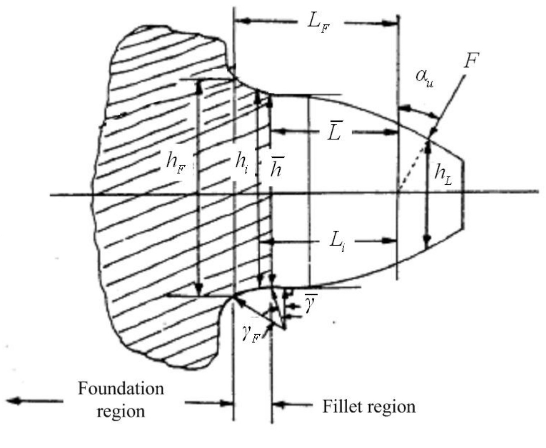

Figure 6 The effective fillet angle and effective fillet length

Foundation Deflection

The foundation deflection δ_F is a function of effective fillet angle γ_F as shown in Fig. 6. It is also given as

$$\delta_F = \frac{F\cos^2\alpha_u}{WE_e}\left\{\frac{16.67}{\pi}\left(\frac{L_F}{h_F}\right)^2 + 2\left(1-\nu\right)\left(\frac{L_F}{h_F}\right) + 1.534\left(1 + \frac{\tan^2\alpha_u}{2.4\left(1+\nu\right)}\right)\right\} \tag{39}$$

where L_F and h_F are effective fillet length and effective fillet height and they are formed as

$$\begin{aligned} L_F &= \bar{L} + r\left(\sin\gamma_F - \sin\bar{\gamma}\right) \\ h_F &= \bar{h} + 2r\left(\cos\bar{\gamma} - \cos\gamma_F\right) \end{aligned} \tag{40}$$

Additionally, the O'Donnell coefficient in Eq. (39) is given as 16.67 and 1.534. γ_F is assumed the constant with the value of 75° which is given in the reference [10].

Hertz Contact Deflection

Figure 7 represents the parameters of Hertz contact deflection δ_H

$$\delta_H = \frac{4F\left(1-\nu^2\right)}{\pi E_{12}W}\left[\ln\left(\frac{2\sqrt{\bar{h}_p\bar{h}_g}}{b}\right) - \left(\frac{\nu}{2\left(1-\nu\right)}\right)\right] \tag{41}$$

where

$$\begin{aligned} E_{12} &= \left(E_{e1} + E_{e2}\right)/2 \\ b &= \left\{\frac{8F}{\pi W}\left(\frac{1-\nu^2}{E_{12}}\right)\Big/\left[\frac{1}{r_p} + \frac{1}{r_g}\right]\right\}^{\frac{1}{2}} \\ r_p &= \left(r_b\right)_p\tan\alpha_k,\ h_p = \left(x_{Fi}\right)_p\sec\alpha_u \\ r_g &= \left(r_b\right)_g\tan\alpha_k,\ h_g = \left(x_{Fi}\right)_g\sec\alpha_u \end{aligned} \tag{42}$$

$\left(r_b\right)_p$ and $\left(r_b\right)_g$ are base radius of pinion and gear, b is the Hertz half contact width. To obtain the total deflections of single tooth, the equivalent elastic modulus E_e in Eqns. (34), (35), (39) and (41) are defined first. According to the reference [10], a tooth is defined to be a wide tooth if it satisfies the following criterion.

$$W/Y > 5 \tag{43}$$

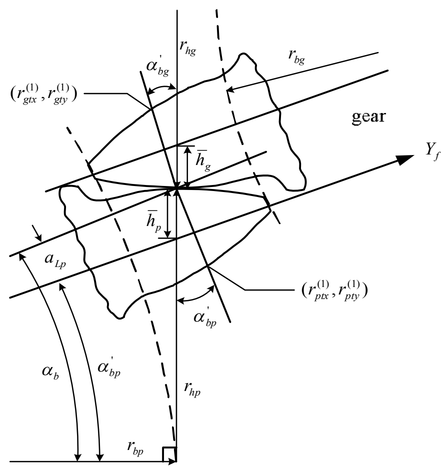

Figure 7 Nomenclature for local compliance

where Y is the tooth thickness at the pitch point. For the case of wide tooth, E_e is the equivalent elastic modulus for the approximated plain strain of tooth deformation.

Finally, substituting Eqns. (34), (35), (39) and (41) into Eq. (29), the total deflections of single tooth can be calculated.

Mesh Stiffness

The mesh stiffness of single tooth can also be derived using the following formula.

$$k_s(t) = \frac{F}{\delta_{total}(t)} \tag{44}$$

If many teeth mesh at the same time, the stiffness can be added by applying a parallel spring model. The dimensionless mesh stiffness $\bar{K}_s$ is represented as

$$\bar{K}_s = \frac{k_s(t)}{|k_s(t)|} = a_4(\varepsilon)^4 + a_3(\varepsilon)^3 + a_2(\varepsilon)^2 + a_1(\varepsilon) + 1 \tag{45}$$

and the indiscriminate length on contact length is defined as

$$\varepsilon = \frac{\phi_d}{\phi_e - \phi_s}\varepsilon_0 \tag{46}$$

where 1, a_1, a_2, a_3 and a_4 are coefficients of curve fitting. ε_0 is the contact ratio and defined as $\varepsilon_0 = l/t_b$, in which l is contact length and t_b is base pitch. ϕ_s and ϕ_e are starting contact angle and ending contact angle of pinion. ϕ_d is represented the difference between the angle of relative meshing position and ending contact angle which can be presented as following.

$$\phi_d = \mathrm{mod}((\phi_0 + \omega_p)/(\phi_e - \phi_s)) \tag{47}$$

The symbol mod( ) represents the remainder of $(\phi_0 + \omega_p)/(\phi_e - \phi_s)$, where ϕ_0 is initial mesh angle of pinion, and ω_p is angular velocity of pinion.

According to the contact ratio ε_0, a low contact ratio gear pair is one for which

$$\varepsilon_0 < 2 \tag{48}$$

In that case, the dimensionless total mesh stiffness $\bar{K}_m$ can be expressed as following.

$$\bar{K}_m(\varepsilon) = \begin{cases} \bar{K}_s(\varepsilon) + \bar{K}_s(1+\varepsilon) & (\varepsilon = 0 \sim q) \\ \bar{K}_s(\varepsilon) & (\varepsilon = q \sim 1) \\ \bar{K}_s(\varepsilon) + \bar{K}_s(1-\varepsilon) & (\varepsilon = 1 \sim 1+q) \end{cases} \tag{49}$$

For the high contact ratio gear pair, the dimensionless total mesh stiffness $\bar{K}_m$ can be expressed as following.

$$\bar{K}_m(\varepsilon) = \begin{cases} \bar{K}_s(\varepsilon) + \bar{K}_s(1+\varepsilon) + \bar{K}_s(2+\varepsilon) & (\varepsilon = 0 \sim q) \\ \bar{K}_s(\varepsilon) + \bar{K}_s(1+\varepsilon) & (\varepsilon = q \sim 1) \\ \bar{K}_s(\varepsilon) + \bar{K}_s(1-\varepsilon) + \bar{K}_s(2-\varepsilon) & (\varepsilon = 1 \sim 1+q) \end{cases} \tag{50}$$

where q is decimal part of contact ratio.

Ⅳ. NUMERICAL RESULTS AND DISCUSSIONS

To verify the proposed procedure using rack cutter to obtain the time-varying mesh stiffness including the modification coefficient, a single degree-of-freedom gear model is studied first. The numerical results of this study are compared with the periodic motions and frequencies have the same trend with reference [6] and Λ defined as $Z_1\Omega/\omega_c$.

As expressed in Eq. (9), the modification coefficients x_p for pinion tooth and x_g for gear tooth are chosen to be larger than x_u to avoid the undercut of tooth and less than x_t to avoid producing the acute top of tooth profile. The single mesh stiffness and the total mesh stiffness of the gear system with different modification coefficients are investigated. Figures 10(a-1) to (a-3) show the mesh stiffness of the single tooth with different modification coefficients. Figures 10(b-1) to (b-3) show the total mesh stiffness of the gear system with different modification coefficients. The lower figures show the mesh stiffness curves for every meshing tooth while the upper figures show the superposition of the curves in the lower figures. The superposition curve is the total mesh stiffness. It is shown from Figs. 10(a-1) to (a-3) that the mesh stiffness varies with contact position and the maximum value occurs near the middle position. The mesh stiffness values in Fig. 10(a-1) are larger than those in Figs. 10(a-2) and (a-3). The curve with the largest mesh stiffness occurs at $x_p = 0.7$, $x_g = 0$ which is the largest positive modification coefficient in the studied cases. It may be explained that the larger modification coefficient brings about thick thickness of tooth and thus induces larger mesh stiffness. From Figs. 10(b-1) to (b-3), the largest total mesh stiffness also found at the largest positive modification coefficient.

The bifurcation diagram is established using Runge-Kutta method. The bifurcation diagrams of the case without modification coefficient effect are shown in Figs. 11.1. It is shown that there are harmonic, sub-harmonic, and chaotic motions. Bifurcation and jump phenomena are also found. The motions at some Λ in the bifurcation diagram are investigated further in Figs. 11.2-11.4. They include four plots: (a) steady state response, (b) frequency spectrum, (c) phase plane, and (d) Poincaré map. The motion at $\Lambda = 1$ is shown in Fig. 11.2. The plots show that it is a harmonic motion (1T motion). Fig. 11.3 shows the motion at $\Lambda = 0.85$. From the plot (b), there are two peaks located at harmonic and sub-harmonic frequencies. There are two loops in the phase plane and two points in Poincaré map. It is known that the motion at $\Lambda = 0.85$ is a sub-harmonic motion (2T motion). In addition, a chaotic motion at $\Lambda = 0.75$ is investigated in Fig. 11.4. The four plots: (a) the time history is non-periodic (b) continuous frequency spectra is found, (c) many loops are shown in the phase plane, and (d) many points locate in Poincaré map.

Table 1 The designed parameters where the center distance can be changed

Parameters	Symbol	Gear 1	Gear 2
Number of tooth (dimensionless)	Z_i	36	36
Modules (mm)	m	3	
Pressure angle (degrees)	α_c	20	
Addendum (mm)	h_f	$1.25\times m$	
Dedendum (mm)	t_f	$1.0\times m$	
Clearance (mm)	h_f	$0.25\times m$	
Tooth width (mm)	W	25.4	
Backlash (mm)	b	3×10^{-5}	
Elastic modules ($\mathrm{N/mm^2}$)	E	2.1×10^5	
Poisson's ratio (dimensionless)	ν	0.3	
Torque (N-mm)	T	100	

Effects of Modification Coefficients

The nonlinear dynamic analysis of a multi-gear train without the modification coefficient effect had been studied by the authors [13]. In this study, the modification coefficient effect is taken into account. The fixed center distance cases are investigated first. There are four cases listed in Table 2. For the four cases, the center distances are fixed since the sum of the modification coefficients x_p for pinion tooth and x_g for gear tooth is zero. The contact ratio influences the total mesh stiffness and the total mesh stiffness plays an important role on the nonlinear dynamic behavior of the gear train system. So the contact ratio and maximum stiffness of single tooth for the four cases are also calculated and listed in Table 2. It is seen that while the modification coefficient of the pinion increases and the modification coefficient of the gear decreases, the contact ratio and the maximum stiffness of pinion and gear decrease, simultaneously. Figures 12 (a)-(c) show the bifurcation diagrams with different modification coefficient under the condition of fixed center distance. The harmonic, sub-harmonic, and chaotic motions are found in the diagrams. The bifurcation and jump phenomena are also found. From Figs. 11 and 12, it is known that the nonlinear dynamic behaviors are different for the cases without and with the modification coefficient effect. Comparing Figs. 12 (a)-(c), it is seen that the chaos region changes with the different modification coefficient. Especially, the chaos region at high frequency moves to the left as the modification coefficient of pinion increases. Consequently, the region of the harmonic motion also changes.

Table 2 The setting value of fixed center distance and the result of the contact ratio and maximum stiffness.

Case No.	x_p	x_g	Contact ratio	Maximum stiffness
1	0	0	1.6780	0.8577
2	+0.1	-0.1	1.6765	0.8539
3	+0.4	-0.4	1.6537	0.7589
4	+0.7	-0.7	1.6018	0.6908

Table 3 shows the cases of variable center distances with changing the modification coefficient of pinion and keeping the modification coefficient of gear to be zero. It is seen that while the modification coefficient of pinion decreases and the modification coefficient of gear remains zero, the contact ratio increases and the maximum stiffness decreases. The bifurcation diagrams for the cases of variable center distances are also drawn in Figs. 13 (a)-(d). The modification coefficients for the four figures are of $x_g=0$ and (a) $x_p=+0.7$ (b) $x_p=+0.4$ (c) $x_p=-0.4$ (d) $x_p=-0.7$. From the diagrams, it is seen that negative modification coefficient may suppress the chaos region for high frequency region. When $x_p=-0.7$ is used, the considered region is improved to be almost harmonic and sub-harmonic motions. From Table 3, it is seen that the contact ratio is the largest and the maximum stiffness is the smallest when $x_p=-0.7$. Thus, the nonlinear effect is insignificant when the maximum stiffness is small.

Table 3 The setting value of variable center distance and the result of the contact ratio and maximum stiffness.

Case No.	x_p	x_g	Contact ratio	Maximum stiffness
1	+0.7	0	1.5583	1.0656
2	+0.4	0	1.5991	0.9588
3	+0.1	0	1.6552	0.8883
4	0	0	1.6780	0.8577
5	-0.1	0	1.7034	0.8259
6	-0.4	0	1.7992	0.7262
7	-0.7	0	1.9405	0.6214

V. CONCLUSIONS

In this study, a procedure which uses the profile of gear tooth and compliance method to obtain the real mesh stiffness is proposed. The influence of modification coefficient on nonlinear dynamic behavior by applying the time-varying stiffness is investigated. Some results based on the numerical analysis are summarized as follows.

The mesh stiffness varies with contact position and the maximum value occurs near the middle position. Using large positive modification coefficient induces the large mesh stiffness. To study the contact ratio and the mesh stiffness, two kinds of cases are studied. For the fixed center distance cases, while the modification coefficient of pinion increases and the modification coefficient of gear decreases, the contact ratio and the maximum stiffness of pinion and gear decrease, simultaneously. For the cases of variable center distances with changing the modification coefficient of pinion and keeping the modification coefficient of gear to be zero, it is seen that while the modification coefficient of pinion decreases and the modification coefficient of gear remains zero, the contact ratio increases and the maximum stiffness decreases.

To gain an insight into the nonlinear dynamic behaviors, the bifurcation diagram, time history, frequency spectrum, phase plane, and Poincaré map are applied. For the gear motion of the system with time-varying mesh stiffness, it is found that harmonic, sub-harmonic, and chaotic motions are found. The bifurcation and jump phenomena are also seen in the bifurcation diagram. For the studied examples of fixed center distance, the chaos region in the bifurcation diagram changes with the different modification coefficient. Especially, the chaos region at high frequency moves to the left as the modification coefficient of pinion increases. For the cases of variable center distance with changing the modification coefficient of pinion and keeping the modification coefficient of gear to be zero, it is seen that negative modification coefficient may suppress the chaos region especially for high frequency region.

ACKNOWLEDGEMENT

The authors are very thankful to the National Science Council of Taiwan for the grant NSC 99-2221-E-194-012 to carry out this project.

VI. REFERENCES

[1] H.N. Ozguven and D.R. Houser, 1988, "Mathematical models used in gear dynamics- a review", *Journal of Sound and Vibration*, **121**, No. 3, pp. 384-414.

[2] A. Kahraman, and R. Singh, 1990, "Non-linear dynamics of a spur gear pair", *Journal of Sound and Vibration*, **142**, No. 1, pp. 49-75.

[3] A. Kahraman, and R. Singh, 1991, "Non-linear dynamics of a geared rotor-bearing system with multiple clearances", *Journal of Sound and Vibration*, **144**, No. 3, pp. 469-506.

[4] O.S. Sener, and H.N. Ozguven, 1993, "Dynamic analysis of geared shaft systems by using a continuous system model", Journal of Sound and Vibration, **166**, No. 3, pp. 539-556.

[5] G. Litak, and M.I. Friswell, 2003, " Vibration in gear systems", Chaos, Solitons and Fractals, **16**, No. 5, pp. 795-800.

[6] A. Al-shyyab, and A. Kahraman, 2005, "Non-linear dynamic analysis of a multi-mesh gear train using multi-term harmonic balance method: sub-harmonic Motions", Journal of Sound and Vibration, **279**, pp. 417-451.

[7] A. Al-shyyab, and A. Kahraman, 2005, "Non-linear dynamic analysis of a multi-mesh gear train using multi-term harmonic balance method: period-one motions", Journal of Sound and Vibration, **284**, pp. 151-172.

[8] Y. X. Zhao and S. Q. Sun, 2008, "Chaotic and bifurcation of gear transmission mechanism", MACHINERY DESIGN & MANUFACTURE/China., **12**, pp. 103-105.

[9] R.W. Cornell, and W.W. Westervelt, 1978, "Dynamic tooth loads and stressing for high contact ratio spur gear", Journal of Mechanical Design, **100**, pp. 69-76.

[10] R.W. Cornell, 1981, "Compliance and stress sensitivity of spur gear teeth", *Journal of Mechanical Design*, **103**, pp. 447-459.

[11] K.Y. Yoon, and S.S. Rao, 1996, "Dynamic load analysis of spur gears using a new tooth profile", Journal of Mechanical Design, **118**, pp. 1-6.

[12] Fakher. Chaari, Tahar Fakhfakh and Mohamed Haddar, 2009, "Analytical modelling of spur gear tooth crack and influence on gearmesh stiffness", European Journal of Mechanics A/Solids, **28**, pp. 461-468.

[13] T. N. Shiau, J. R. Chang, K. H. Huang and C. J. Cheng, 2010, "Bifurcation and Chaotic Motion of A Multi-Mesh Gear Train with Time-Varying MESH Stiffness Application of Rack Cutter," International Gas Turbine Institute ASME TURBO EXPO 2010, Paris, France

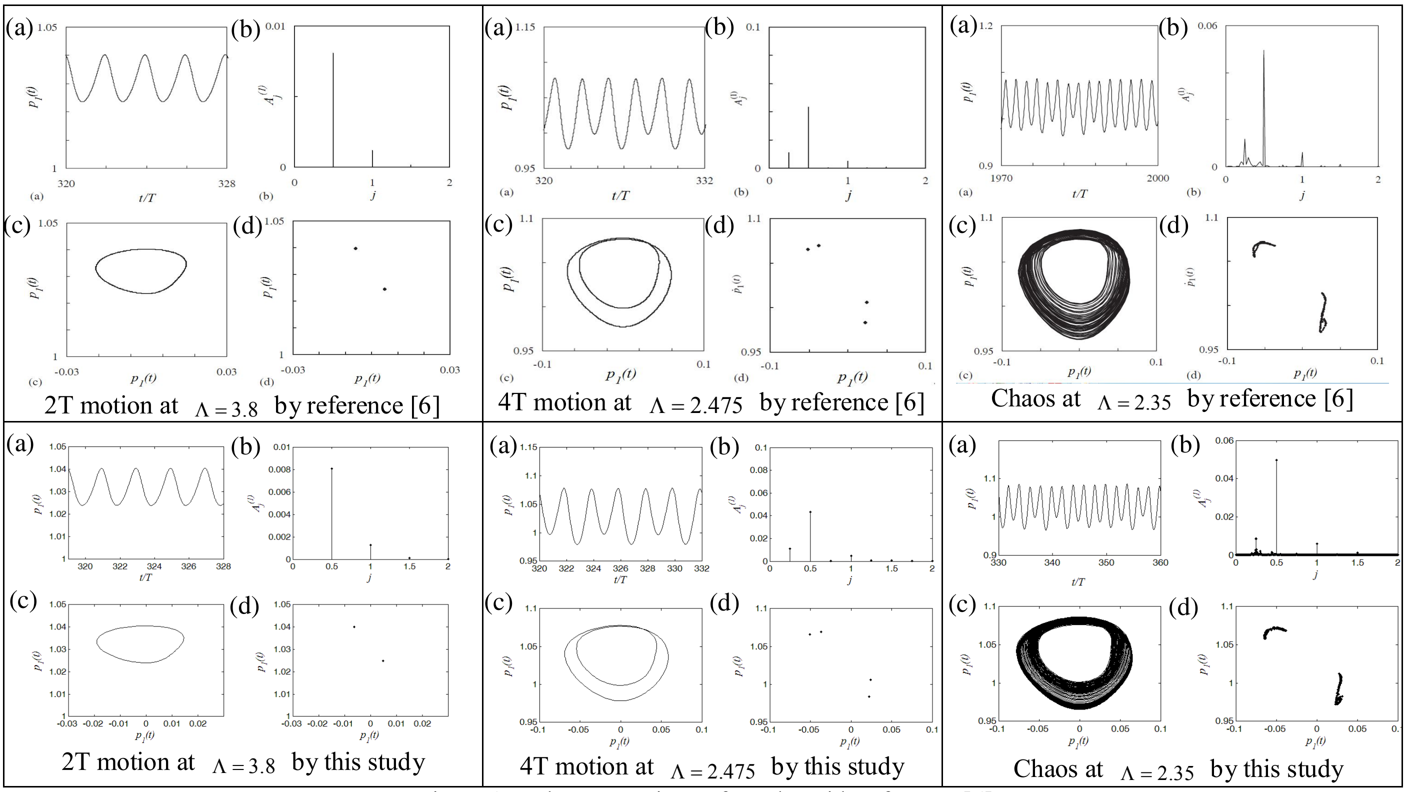

Figure 9 The comparison of results with reference [6]

(a) steady state response $\bar{p}_1(\bar{t})$, (b) frequency spectrum, (c) phase plane plot, (d) Poincaré map.

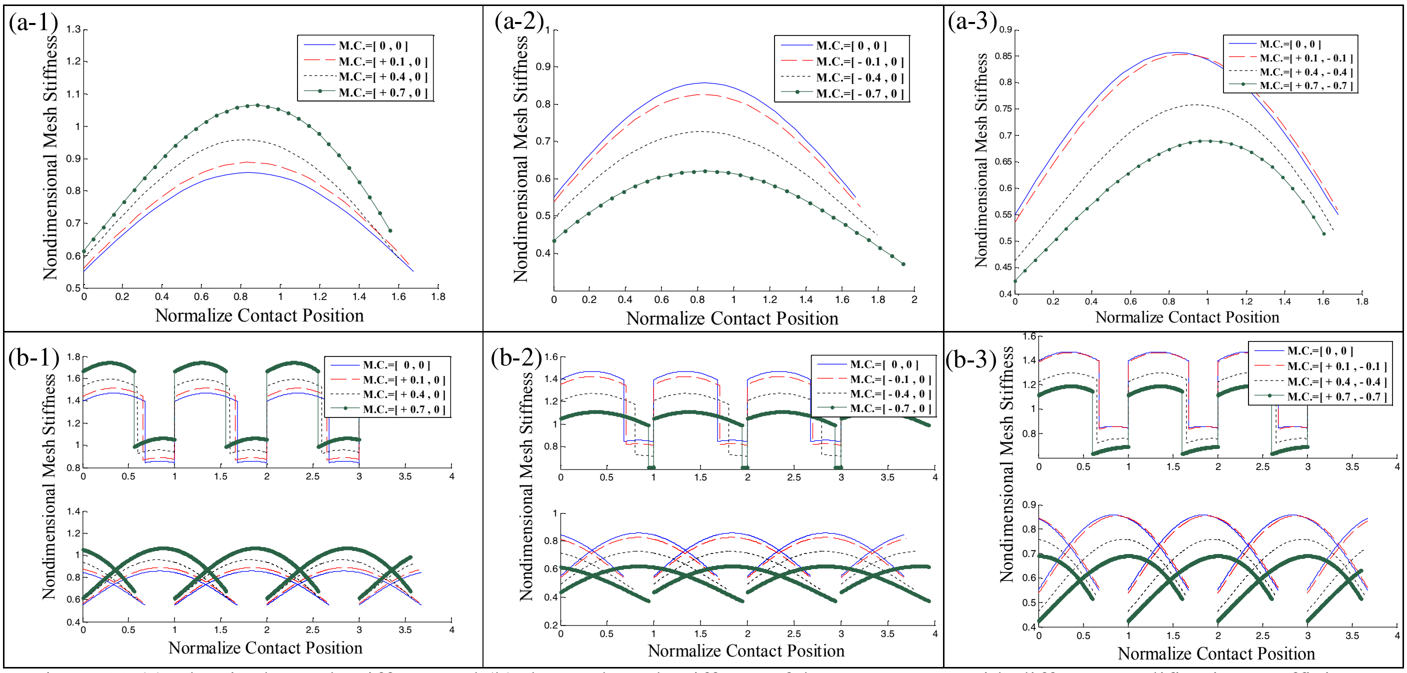

Figure 10 (a) The single mesh stiffness and (b) the total mesh stiffness of the gear system with different modification coefficients. *M.C.=[+0.1, 0] means $x_p = 0.1$ and $x_g = 0$.

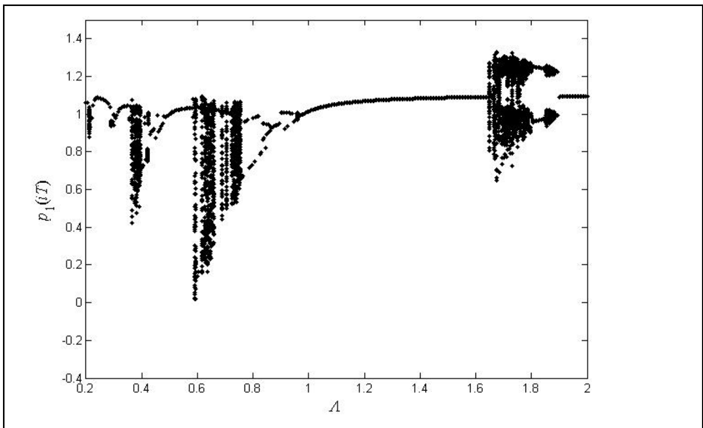

Fig. 11.1 Bifurcation diagram of nT and chaotic motions within $\Lambda \in [\,0.2,\ 2\,]$, $x_p = x_g = 0$, $\varsigma = 0.03$

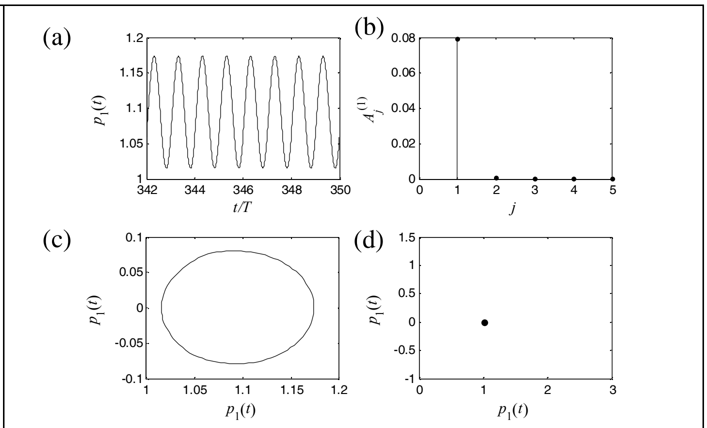

Fig. 11.2 1T motion at $\Lambda = 1$ (a) steady state response $\bar{p}_1(\bar{t})$, (b) frequency spectrum, (c) phase plane plot, (d) Poincaré map.

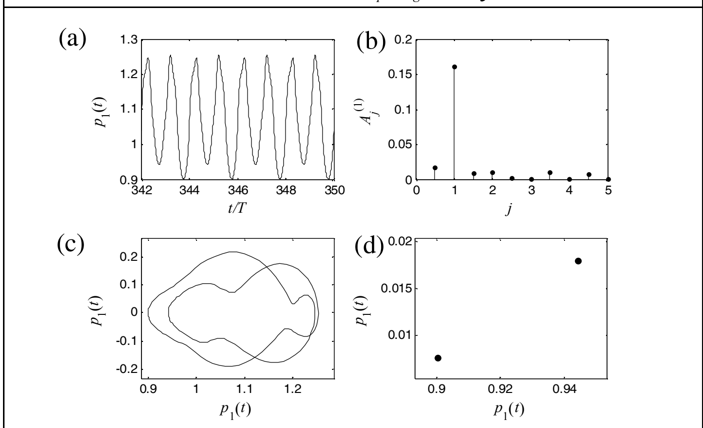

Fig. 11.3 2T motion at $\Lambda = 0.85$ (a) steady state response $\bar{p}_1(\bar{t})$, (b) frequency spectrum, (c) phase plane plot, (d)Poincaré map.

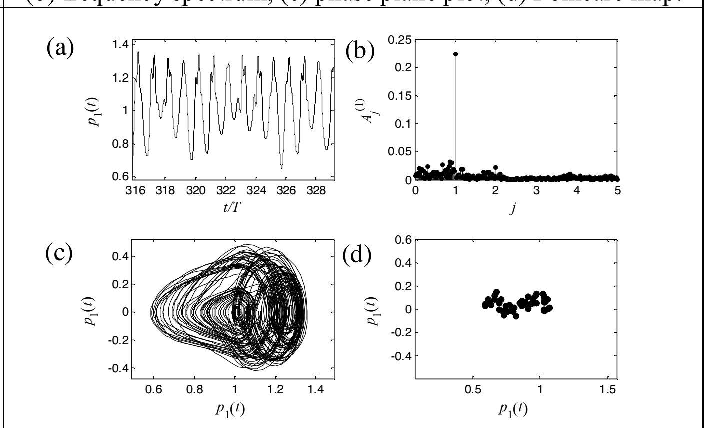

Fig. 11.4 Chaotic motion at $\Lambda = 0.75$ (a) steady state response $\bar{p}_1(\bar{t})$, (b) frequency spectrum, (c) phase plane plot, (d) Poincaré map.

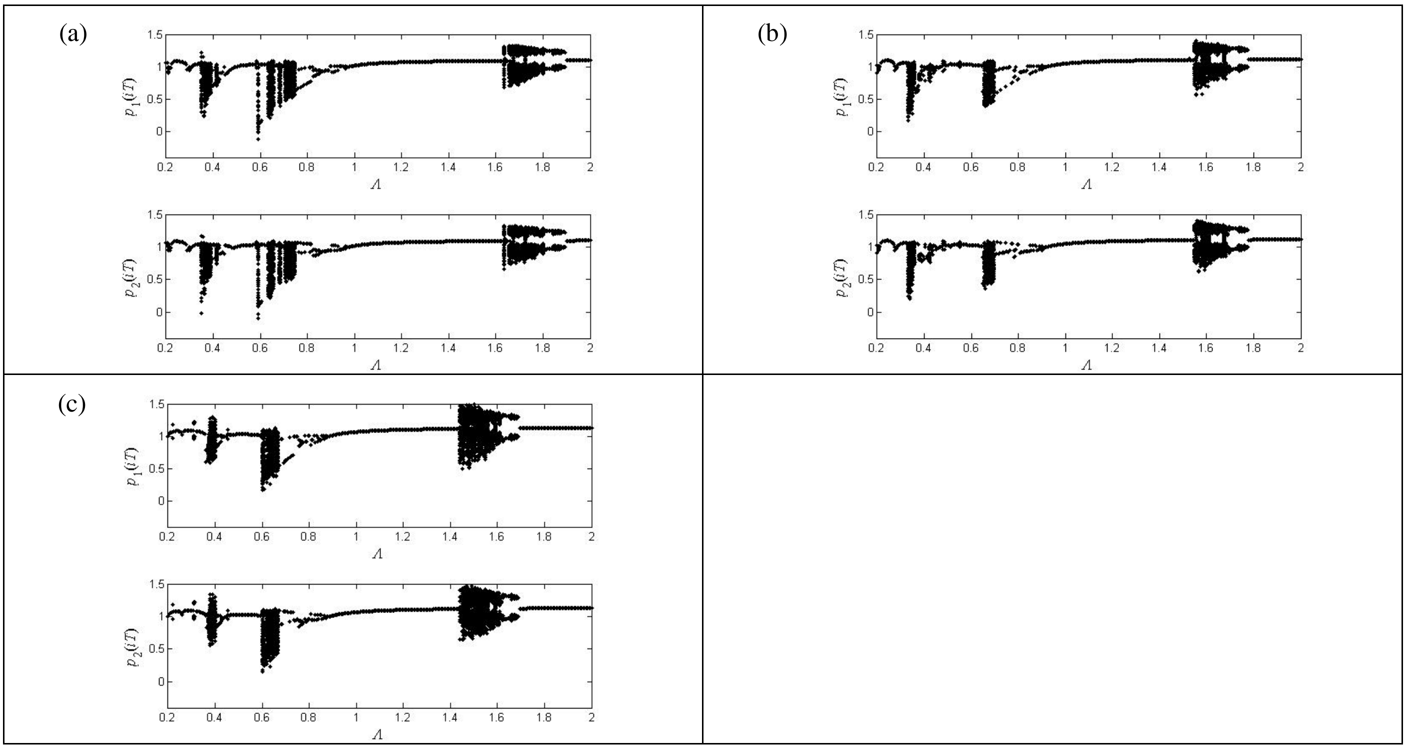

Fig. 12 Bifurcation diagram of nT and chaotic motions within (a) $\Lambda \in [\ 0.2,\ 2\ ]$ $x_p = +0.1,\ x_g = -0.1$, $\varsigma = 0.03$ (b) $\Lambda \in [\ 0.2,\ 2\ ]$ $x_p = +0.4,\ x_g = -0.4$, $\varsigma = 0.03$ (c) $\Lambda \in [\ 0.2,\ 2\ ]$ $x_p = +0.7,\ x_g = -0.7$, $\varsigma = 0.03$

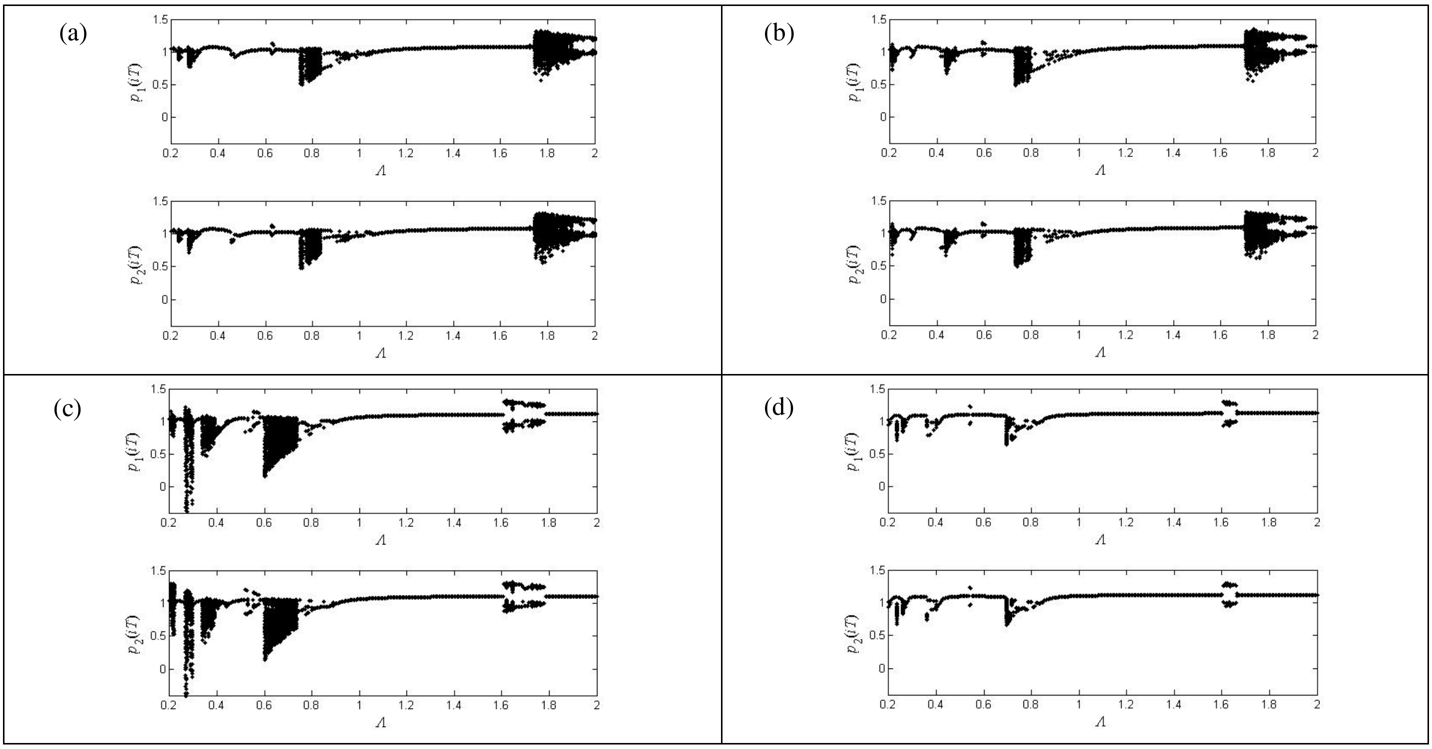

Figure 13 Bifurcation diagram of nT and chaotic motions within $\Lambda \in [\ 0.2,\ 2\ ]$, $\varsigma = 0.03$, x_g=0 and (a) $x_p = +0.7$ (b) $x_p = +0.4$ (c) $x_p = -0.4$ (d) $x_p = -0.7$

NOMENCLATURE

A_i	:	Cross-section of i^{th} element
b	:	Hertz-contact half width
b_c	:	Characteristic width
C	:	Total compliance
$c_1(t)$, $c_2(t)$	:	Gear mesh damping value
c_k	:	Clearance
c_p, c_g		displacements of center distance
E_e	:	Equivalent elastic modulus
F_L	:	Applied load
$f(t)$	:	External force
$g_1(t)$, $g_2(t)$	:	Discontinuous displacement function
h_f	:	Effective fillet height
I_i	:	Polar mass moment of inertia
$\vec{i}, \vec{j}, \vec{k}$	:	Unit coordinate vector
$[K]$	:	Stiffness matrix
$\bar{K}_m$	:	Total dimensionless mesh stiffness
$\bar{K}_s$	:	Dimensionless mesh stiffness
$k_1(t)$, $k_2(t)$	:	Gear mesh stiffness
L_F	:	Effective fillet length
$[M_{21}], [M_{2f}], [M_{f1}]$, $[L_{21}]$	:	Transformation matrix between different coordinates
N_1, n_1	:	Normal vector and unit normal vector
q	:	Decimal part of contact ratio
$p_1(t)$, $p_2(t)$	:	Dynamic transformation error
r_p		Radius of pitch circle
r_{bi}	:	Radius of base circle
r_{op}, r_{og}		Radii of pitch circle
$\mathbf{r}_{fp}^{(1)}$		Tooth profile vector of pinion
$\mathbf{r}_{fg}^{(1)}$		Tooth profile vector of gear
s_o	:	Length of contact
t	:	Real time
$\bar{t}$	:	Dimensionless time
t_e	:	Base pitch
t_f	:	Dedendum
t_o	:	Standard pitch
$T_i(t)$	:	torque
u_1	:	Straight line section parameter of rack cutter
W	:	Tooth width
Z_i	:	Number of gear mesh
α	:	Pressure angle
α_b	:	Mesh pressure angle
Λ	:	Rotating speed/the first natural frequency
ρ	:	Radius of fillet
θ_1	:	Arc section parameter of rack cutter
$\theta_i(t)$	:	Rotational displacement
δ_H	:	Hertz contact deflection
ε	:	Indiscriminate length on contact length
ε_o	:	Contact ratio
ω_c	:	Characteristic frequency
ζ	:	Damping ratio
$\kappa_1(\bar{t})$, $\kappa_2(\bar{t})$	:	Dimensionless mesh stiffness
ϕ	:	Rotation angle